Advances in Complex Systems
Vol. 25, No. 7 (2022) 2250009 (24 pages)

DOI: 10.1142/S0219525922500096

World Scientific
www.worldscientific.com

LONG-RANGE CONNECTIONS, REAL-WORLD NETWORKS AND RATES OF DIFFUSION

TANYA ARAÚJO
REM/UECE - ISEG, Universidade de Lisboa,
1249-078 Lisboa, Portugal
tanya@iseg.ulisboa.pt

R. VILELA MENDES*
CMAFCIO, Universidade de Lisboa,
1749-016 Lisboa, Portugal
rvilela.mendes@gmail.com; rvmendes@fc.ul.pt

Received 5 April 2022
Revised 5 September 2022
Accepted 8 October 2022
Published 9 November 2022

Long-range connections play an essential role in dynamical processes on networks, on the processing of information in biological networks, on the structure of social and economical networks and in the propagation of opinions and epidemics. Here, we review the evidence for long-range connections in real-world networks and discuss the nature of the nonlocal diffusion arising from different distance-dependent laws. Particular attention is devoted to the characterization of diffusion in finite networks for moderate large times and to the comparison of distance laws of exponential and power type.

Keywords: Networks; long-range connections; anomalous diffusion.

1. Introduction

Long-range connections play an important role in the dynamical processes on networks. For example, existence and relevance of long-range connections in the brain has been studied [1–6] with diminished long-range functional connectivity being associated to cognitive disorders [7]. Long-range connections are also important for the structure of social and economic networks [8–10] as well as for the propagation of epidemics [11].

Dynamics on networks involving jumps over many links or cascades of many unit jumps may lead to anomalous diffusion [12–16]. Likewise, the existence of long-range connections is expected to lead to anomalous diffusion effects. When the density of long-range connections follows a power law, as a function of a suitably defined

* Corresponding author.

distance, the propagation of signals in the network behaves as the solution of a fractional diffusion equation [17, 18].

Because networks with power-law connections, leading to superdiffusion, display properties very different from scale-free and hub-dominated networks, it has been proposed to classify them as a new network class, *the fractional networks*.[a] However, it is to be expected that the nature of the diffusion and therefore the propagation of information in the network, may be different for other distance dependencies of the density of long-range connections. This is an important issue because, for example in brain networks, existence of long-range connections between the specialized modules does not guarantee global integration of the cognitive functions. It is also necessary that the flow of information be sufficiently fast for the stimulus integration to be performed in a timely manner.[b]

Networks where nodes and edges are embedded in a metrical space have been considered before and reviewed in [19]. The emphasis of the vast majority of previous works has been on their topological properties, degree distribution, communities, motifs and degree correlations. Here, instead, we emphasize the distance-dependency laws of connection strengths, in particular for long-range connections, as well as the impact that these laws have on the propagation of information in the networks. In Sec. 2, analyzing the data of several networks, we find clear evidence for the existence and importance of long-range connections in real-world networks. The main focus is the extraction of the distance-dependent functional laws of the connections. A general result that is obtained in many networks is that short-distance and long-distance connections follows different laws. This is consistent with the modular nature of many networks, which have a high density of connections inside local modules and a much smaller number of long-range connections. This is typically the structure of brain networks. In these networks, the long-range connections between the modules favor integration of perception but, on the other hand, they also imply a much larger biological cost. As we find out, this two-laws behavior also appears in a transport network, again signaling a modular structure on the economic organization of society. In social networks the laws for short- and long-range connections are more uniform. Probably, it reflects the fact that short- and long-range connections have similar costs. As a guiding principle we have compared the long-distance distance functional laws with both exponential and power-law functions. Note that whether or not scale-free networks (in the sense of the degree distribution) are abundant in Nature [20], power laws in the distance dependency of the long-range connections intensity seem to play an important role in a fair amount of real-world networks.

Propagation of a material entity or a signal in a network with long-range connections may be framed as a problem of nonlocal diffusion. A number of theoretical results and characterization of general features already exist for nonlocal diffusion

[a] Networks with nonfractional couplings where nevertheless diffusion has fractional features, not to be confused with fractionally coupled networks [26, 27].

[b] This seems of particular relevance for the forward and backwards loops in the predictive coding mode of brain operation.

[21–23]. An important result is the behavior of the propagating signal for large times, because that defines the nature of the network as a collective entity. The existing theoretical results concern the asymptotic $t \to \infty$ behavior. It is well known [21, 24] that for compact support diffusion kernels, the asymptotic behavior is identical to the one of the heat equation (normal diffusion). For finite networks the distribution of the connections intensity has compact support, hence the $t \to \infty$ behavior would be trivial. However, what is important in practice is not the behavior of the propagation of information for extremely large times, but for short and intermediate large times. In Sec. 3, we address this practical important problem by a detailed study of nonlocal diffusion, with particular emphasis on the comparison of the power-law and exponential distance dependence of the connections. We find out that for power laws with a cut-off, the solution behaves for intermediate large times like an anomalous diffusion solution, very different from the asymptotics for extremely large times. Analytical estimates for small and large times are possible, but not for these intermediate times of practical interest. By numerical calculations, we have nevertheless been able to parametrize and quantify the effective "fractionality" of the diffusion for intermediate times.

Power-law and exponential distance dependency of the connections lead to very different diffusion behavior. However, it is many times difficult to distinguish between these two dependencies from the experimental data. To emphasize this point we have displayed for all analyzed networks, both power-law and exponential fits. The reason for this difficulty is further analyzed in Sec. 4 (see Fig. 16).

Finally, in Sec. 4, we carry out a numerical experiment of propagation of a unit signal in power law, exponential and nearest-neighbor networks. The smaller propagation times are, of course, for the power-law networks, but even the exponential network is much more efficient that the nearest-neighbor one. Past studies on the effect of space on processes in networks, has centered on navigability on small-world networks with long-range connections [25]. What our theoretical and simulation results put into evidence is that it is the functional form of the distance law that has the stronger effect on the speed of navigation.

The set of real-world networks that we were able to analyze is of course limited. This was the data that we were able to obtain either from the web or kindly provided by the referenced authors. We encourage the readers that have access to other data to pursue our preliminary work. Interesting questions to explore are the nature of the functional law of connections in the human brain (both structural and functional) as compared to other mammals, as well as the nature of the "fractionality" index across species. Are some brain impairments, that have been identified, related to the nature of the distance-dependency law or just to the overall number of long-distance connections? Data on the more popular social networks and their distance-dependent links is harder to obtain. Interesting studies might be performed in that data when available, correlated also with the diffusion of trends and opinions. Some data on ecological and trophic networks was available, but not sufficient for robust results.

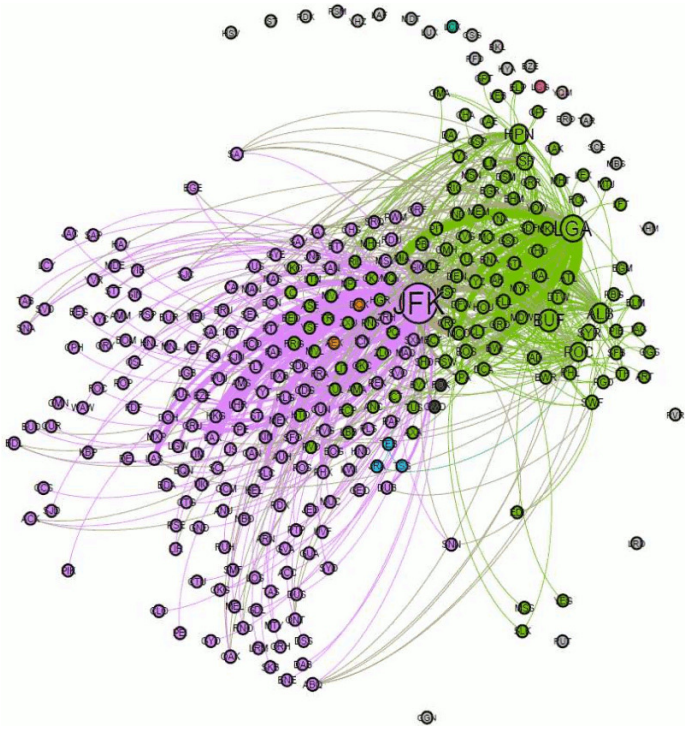

Fig. 1. The network of flights to or from New York airports in January 2019.

Note that in some of these networks the relevant notion of distance not being geographical distance, the identification of the relevant measure is an important issue.

2. Real-World Networks: Analysis of Empirical Data

2.1. *A human mobility network*

The first network that was analyzed was the network of flights to and from airports in the New York region.

Data for the month of January 2019, for example, was collected from the database available in [28]. The file contains the following fields:

Passengers (number of passengers),
Distance (in miles),
Origin_Airport_ID (unique identifier Airport_ID),
Destination_Airport_ID,
Month

From the data in these fields a weighted network of Airport_IDs is defined. The Airport_IDs are the nodes while the strength of the links is given by the number of passengers flying between the nodes (Origin_Airport_ID and Destination_Airport_ID,

or vice versa) during the time interval being considered (month), regardless of the flight direction. Figure 1 shows the network of flights to and from New York airports in January 2019. The network has 317 nodes (airports) and 641 weighted links, the strongest link being a Delta Airline flight that links the airports of LaGuardia (LGA) and Atlanta (ATL). The largest distance (10,201 miles) concerns the JFK airport in New York and the Melbourne Airport, in Australia. The average degree is 4 and the average weighted degree is 98,319. The network diameter is 7 and the network modularity displays four different classes. The colors in Fig. 1 characterize each one of the modularity classes, while the size of each node is proportional to its degree. The average clustering coefficient is 0.49 and the average path length is 2.4.

We have collected the same type of data for the full years of 2019 and 2020. The results are plotted in Figs. 2 and 3.

In these figures, we also make polynomial fits corresponding in the left-hand plots to a power law $w \sim d^{-\beta}$ where w is the number of passengers and d the inter-airports distance and to an exponential law $w \sim \exp(-\lambda d)$ in the right-hand plots. Our conclusion is that the data is better described by a two-law structure separating short- and the long-range connections, with the long-range connections obeying an approximate power law. According to the analysis in Sec. 3, this power law leads to anomalous diffusion, which has relevance for the fast propagation of trends and diseases.

Other authors have also emphasized the role of long-range connections in human mobility networks. For example, Viana and Costa [29] analyzed their role in the

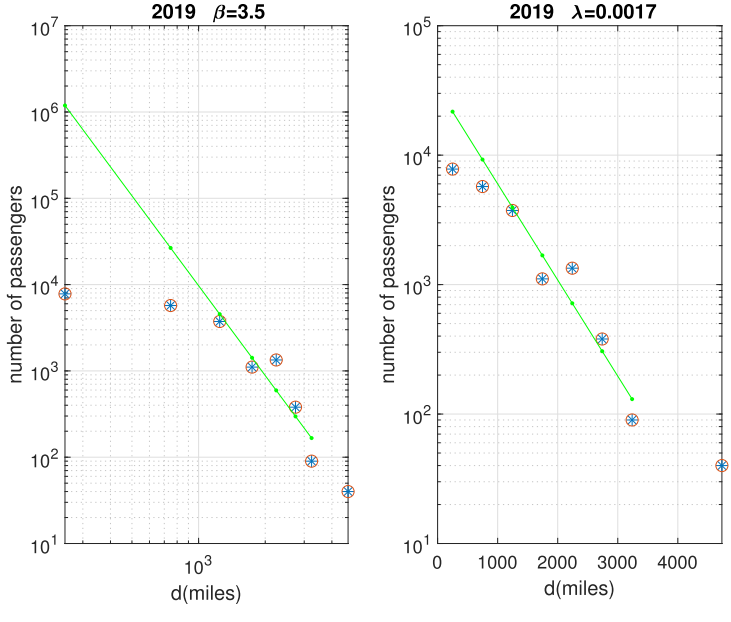

Fig. 2. Distance-dependent distribution of the network links in the airports network for the year 2019. β is the exponent of the power law $w \sim d^{-\beta}$ and λ the coefficient in the exponent of the exponential law $w \sim \exp(-\lambda d)$.

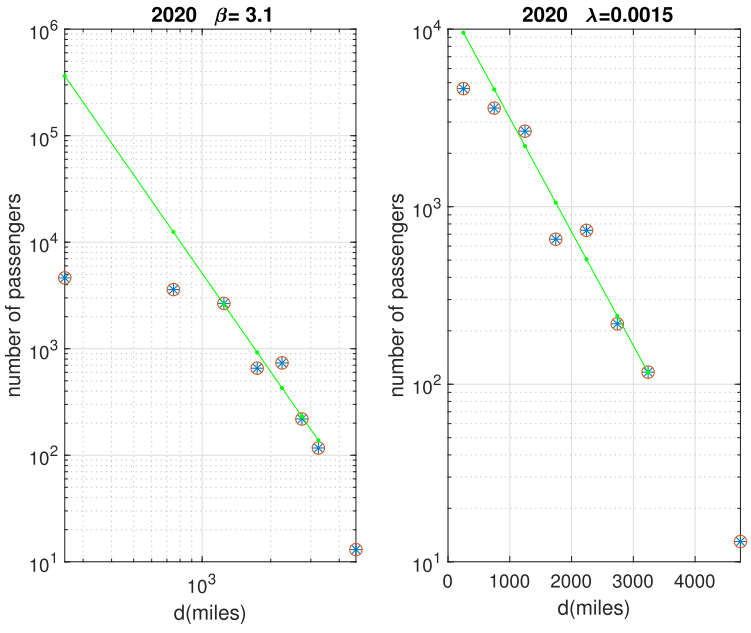

Fig. 3. Distance-dependent distribution of the network links in the airports network for the year 2020. β is the exponent of the power law $w \sim d^{-\beta}$ and λ the coefficient in the exponent of the exponential law $w \sim \exp(-\lambda d)$.

London urban and US highway networks mostly in connection with the small-world properties and travel velocity between nodes. The statistics of travel patterns and returns to the same locations using cell phones has also been studied [30]. The conclusion being that the individual travel patterns collapse into a single spatial probability distribution, it would be interesting to find out whether there are distinguishing features in short- and long-travel distances. Another human mobility that has been analyzed by Riascos and Mateos [31] involved one billion taxi trips in New York City. The conclusion was that the probability of a trip to a site inside a circular region of radius R around the origin is approximately constant, whereas the probability to a long-range trip outside this circle decays as a power law with an exponential cutoff. That is, a modular structure similar to what we have found for the airports network.

2.2. *Brain networks*

Network theory is a valuable tool to explore the complex nature of brain networks, the discovery of patterns of connections between cortical areas being the focus of most research works (see, for example, [32–35]). Our analysis will concentrate on macaque and mouse brain networks.

2.2.1. *Macaque*

The data used here was collected from Core-Net.org [32]. In this data the pathways linking cortical areas have been followed by retrograde tracing experiments using injections of fluorescent retrograde tracers.[c]

The file PNAS2013.xlsx downloaded from the database has the following fields: (1) Monkey, (2) Source area, (3) Target area, (4) Neurons, (5) Fraction of labeled neurons (FLNe), (6) Distance.

Source (j) and target (i) areas are labeled through retrograde labeling using fluorescent tracers [35]. This labeling method reveals all incoming connections j_i to an injected (target) area i by labeling the cell bodies of the neurons in source area j for which their axons connect to area i. The FLNe, given by the ratio $\text{FLNe} = \frac{\text{Neurons}}{\text{Total Neurons}}$, may be interpreted as the probability of a neuronal projection from Source area i to Target area j [36].

The fields Source and Target provide a weighted network of 91 brain areas. The Source and Target areas are the nodes while the intensity of the links corresponds to the number of Neurons connecting these areas. Figure 4 shows the network of the 91

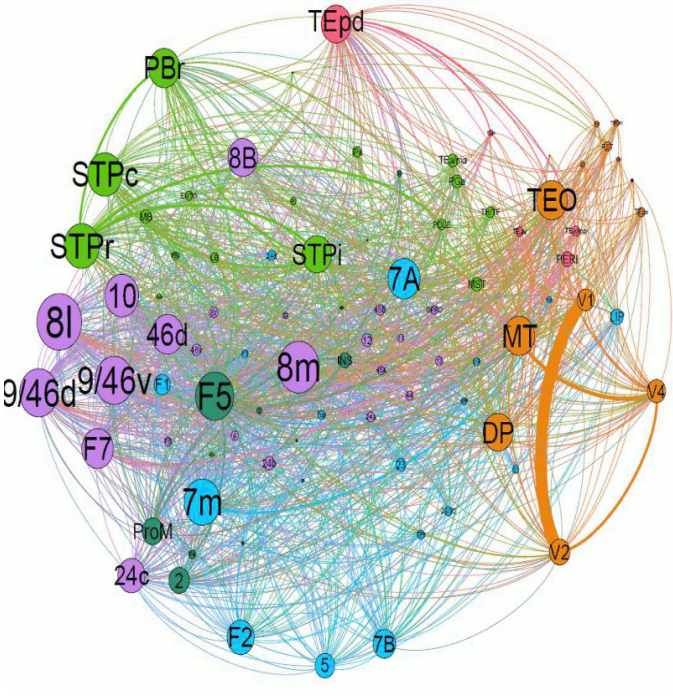

Fig. 4. The network of 91 brain areas collected from 39 macaques.

[c]Localization of injection sites and labeled neurons was based on a new reference atlas that includes 91 cortical areas mapped to the left hemisphere of case M132 [33].

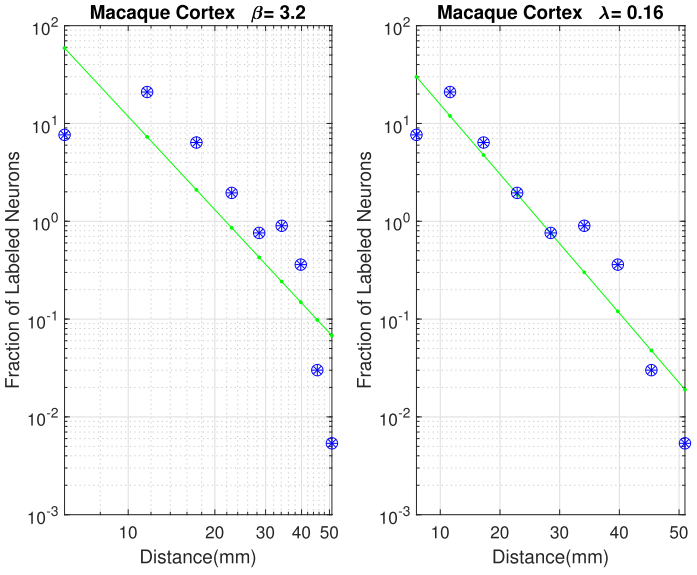

Fig. 5. Distance-dependent distribution of the network links for the macaque cortex. β and λ have the same meaning as before.

areas in the PNAS2013.xlsx file, 39 macaques being sampled in 1989 instances of the database. Thus, this macaque network has 91 nodes, connected by 1401 links, the size of each node being proportional to its degree. The average degree is 30.7 and the average weighted degree is 869,967.3. The network diameter is 3 and the network modularity displays six different classes, characterized by different colors in the figure. The average clustering coefficient is 0.74 and the average path length is 1.6. Note that the data that we analyze refers to connections from 91 different sources to just 29 different target areas. The distance-dependent distribution of the network links is shown in Fig. 5 both in a log–log and a semilog plot.

It seems that in this case the better fit is an exponential one $w = \exp(-\lambda d)$, w being the links intensity (number of Neurons) and $\lambda = 0.16\,\mathrm{mm}^{-1}$.

Likewise, if instead of the Neuron field we focus on the FLNe the result is quite similar, being in accordance with the work in [35], which by using data from macaque and mouse, infers the existence of a general organizational principle based on an exponential distance rule

$$\mathrm{FLNe}(d) = c * \exp(-\lambda d). \tag{1}$$

2.2.2. *Mouse*

The database used here is obtained from [34], MouseDatabase.xlsx. The file MouseDatabase.xlsx contains, among others, the following fields:

(1) Mouse, (2) Source area, (3) Target area, (4) FLNe, (5) Neurons, (6) Distance. The fields Source and Target allow to define a network of 47 brain areas. The Source

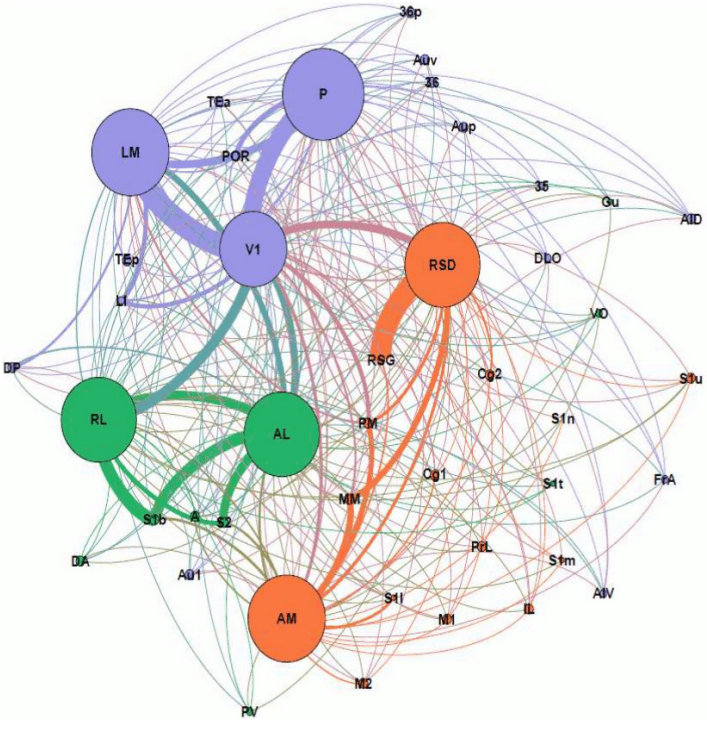

Fig. 6. The network of neurons in 47 brain areas of 27 mice.

and Target areas are the nodes while the links correspond to the number of Neurons between the Source and Target areas, as in the macaque example studied before. Figure 6 shows the network of 47 areas in MouseDatabase.xlsx, where 27 mice were sampled in 1242 instances of the database. The mouse network has 47 nodes and 703 weighted links.

In this mouse example, the number of target areas is much smaller than in the macaque one. There are just seven (AM, AL, RL, P, ML, RDS and V1) target areas (against 43 source ones) and therefore these are the areas with the largest degrees, as Fig. 6 shows. The network diameter is 2 and the network modularity displays three different classes characterized by different colors in Fig. 6. The average clustering coefficient is 0.8 and the average path length is 1.35.

The distance-dependent distribution of the links is shown in Fig. 7. This is a case where it is difficult to decide between an exponential and a power law. For an exponential law we would have $w \sim \exp(-\lambda d)$ with $\lambda = 3.9\,\mathrm{mm}^{-1}$. The average distance in our sample is $\langle d \rangle_{\mathrm{mouse}} = 0.78\,\mathrm{mm}$, smaller than the one reported in the samples analyzed by other authors (for example, $\langle d \rangle_{\mathrm{mouse}} = 4.54\,\mathrm{mm}$ in [34]). The occurrence of an exponential law for the macaque and mouse brain networks is in fact favored by most authors. Note, however, that Knox *et al.* [37] in a high-resolution study of the mouse connectome shows a power-law fit to the normalized connection

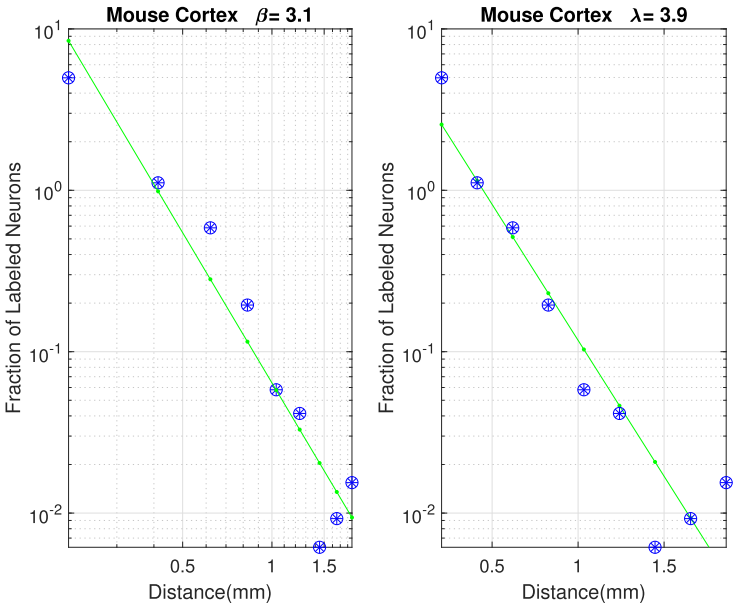

Fig. 7. Distance-dependent distribution of the links in the mouse network. β and λ have the same meaning as before.

density as a function of the distance. The statistics of the data fit is however too poor to be able to decide. It would be interesting to compare the functional laws in the macaque and mouse networks with those of the human brain, both structural and functional, for which we have not yet had access to reliable data.

2.3. *A social network*

Here, we analyze the Brightkite location-based online social network [38]. Brightkite is a location-based social networking service provider where users share their locations by checking-in. This friendship network was collected using users public API, and consists of 58,228 nodes and 214,078 edges. The network is originally directed but later transformed into a network with undirected edges when there is a friendship in both ways. Data include a total of 4,491,143 check-ins of the network users over the period April 2008–October 2010.

The first downloaded file (Loc-brightkite_totalCheckins.txt) with information on the users location contains the fields: (1) User, (2) Latitude, (3) Longitude, (4) Location_id, (5) Check-in time. The second Brightkite file (loc-brightkite_edges.txt) is a friendship network of Brightkite users (58,228 nodes and 214,078 edges).

From the locations of each pair of Brightkite friends the corresponding distance is computed. The characterization of the distance-dependent distribution of the network links (number of friends) is shown in Fig. 8. Figure 8 shows a polynomial fits

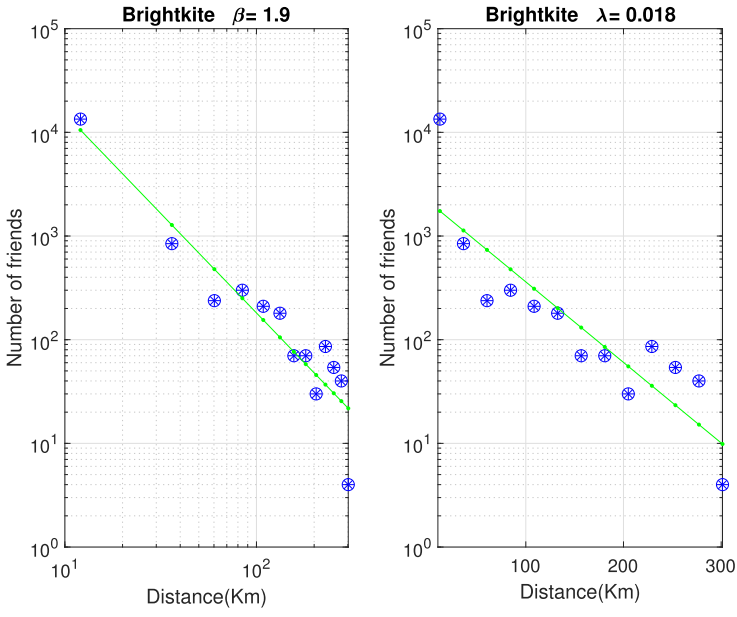

Fig. 8. Friends versus distance in the Brightkite network. β and λ have the same meaning as before.

(in log–log and semilog plots) of the number of friends $w_{i,j}$ and their distances d_{ij}. The best fit corresponds to a power laws $w_{ij} = d_{ij}^{-\beta}$ with $\beta = 1.9$. In this case, one obtains a fairly uniform power law without any indication of a modular structure.

2.4. *A fungi network*

The network studied here is part of a large data set of 269 fungal networks available at [39, 40]. The data providers construct fungal networks by estimating cord conductances. In defining fungal networks, the nodes are located at hyphal tips, branch points and anastomoses, while the edges represent cords. Structural networks are constructed by calculating edge weights based on how much nutrient traffic is predicted to occur along each edge.

Being location-based networks, in addition to the complete list of network links, the data set also includes the coordinates of each node. For the network present here, we used the sample identified as *Pp_M_Tokyo_U_N_26h_1*. This sample has 1357 nodes and 3716 undirect links. From the coordinates of each pair of linked nodes the corresponding distance is computed. The characterization of the distance-dependent distribution of the network links is shown in Fig. 9.

This is again a situation where it is difficult to decide whether to infer an exponential or a power law.

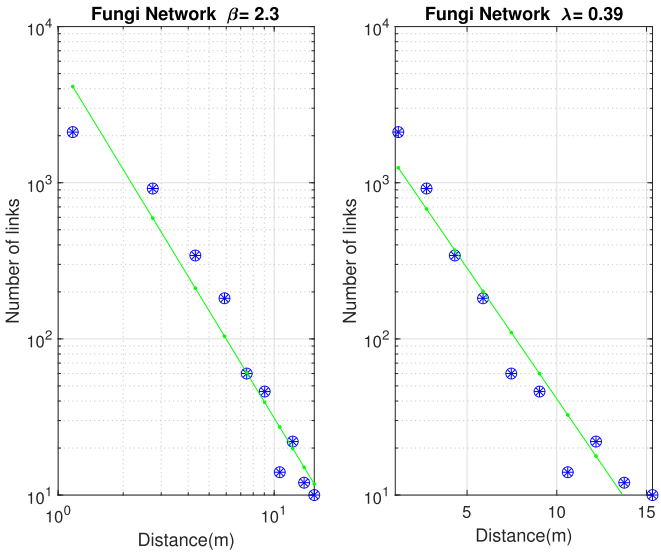

Fig. 9. A fungi network. β and λ have the same meaning as before.

3. Nonlocal Diffusion and Long-Range Network Connections

Short- and long-range connections determine the global behavior of a network, both its emergent dynamical evolution and the spread of information (or pathologies) throughout the network. It is intuitive that long-range connections must play a role on the speed of the spread of information as well as on the context integration of the sensory inputs in brain networks. However, it is not so obvious to infer how such phenomena may depend on the density and distance dependence of the long-range connections.

Here, we make an attempt to address these questions in the framework of the theory of nonlocal diffusion [21–23]. Let some time-dependent quantity (a field) $\phi(t, x)$ stand for the density of individuals, quantity of information or activation in a d-dimensional space X. There are two related problems of nonlocal diffusion. If $\phi(t, x)$ stands for the density of individuals or the degree of activation, the nonlocal diffusion equation is

$$\frac{\partial}{\partial t}\phi(t,x) = \int_X \rho(y,x)\phi(t,y)d^n y - \phi(t,x), \tag{2}$$

$\rho(y, x)$ being the probability density for a jump (or transmission) from y to x and the last term accounts for the rate of departure from x to other locations.

$$-\phi(t,x) = -\int_X \rho(x,y)\phi(t,x)d^n y, \tag{3}$$

because $\int_X \rho(x, y)d^n y = 1$. Equation (2) conserves the quantity $Q = \int_X \phi(t, x)d^n x$. In addition one might consider additional terms added to the right-hand side of these

equations to represent nonlocal internal interactions, localized sources or consumption terms.

However, if $\phi(t, x)$ stands for an information quantity or a disease, the last term might not make sense. Information does not decay in transmission to other nodes nor a disease is cured by infection of the neighbors. To simply suppress the last term in Eq. (2) to describe this situation does not make sense either because then Q grows exponentially. We will come back to this question on our numerical simulations of propagation of an impulse of information and for the time being our analysis will concern Eq. (2).

In the continuous approximation, which would be a good approximation for a network with a very large number of nodes, the kernel $\rho(y, x)$ may be considered to be proportional to the density of connections between nodes at the positions y and x. Here, we will be concerned with the case where the kernel $\rho(y, x)$ is a function of the distance $|y - x|$ only

$$\rho(y, x) = \rho(|y - x|),$$

with the distance defined by a problem-adapted metric. Without loss of generality, we will assume the parametrization of the network to be such that the distances are Euclidean distances on that parametrization.

From our analysis of the real-world networks with long-range connections we have concluded that two important functional distance dependencies are the power law and the exponential law. It is therefore for these two laws that our calculations will be performed. As for dimensionality, two most important cases are $d = 2$ and $d = 3$. However, other higher dimensions may be important as well, when the network nodes are characterized by many parameters. Important examples are social networks, credit scoring networks, etc. Therefore, we will derive general results for arbitrary (finite) dimensions. Our main interest is the asymptotic behavior of $\phi(t, x)$ for long and intermediate times. For $\rho(y, x) = \rho(y - x)$ the integral in (2) is a convolution and a Fourier transform treatment is appropriate

$$\frac{\partial}{\partial t}\tilde{\phi}(t, k) = \tilde{\rho}(k)\tilde{\phi}(t, k) - \tilde{\phi}(t, k), \tag{4}$$

with

$$\begin{aligned} \tilde{\phi}(t, k) &= \int_X e^{ik\cdot x}\phi(t, x)d^n x, \\ \tilde{\rho}(k) &= \int_X e^{ik\cdot x}\rho(y - x)d^n x. \end{aligned} \tag{5}$$

From Eq. (4)

$$\begin{aligned} \tilde{\phi}(t, k) &= \tilde{\phi}(0, k)\exp(t(\tilde{\rho}(k) - 1)), \\ \phi(t, x) &= \frac{1}{(2\pi)^n}\int_{\tilde{X}} e^{-ik\cdot x}\tilde{\phi}(t, k)d^n k. \end{aligned} \tag{6}$$

For definiteness we consider a Cauchy problem corresponding to the diffusion of a unit pulse at the origin at time zero. That is, we are considering what is called the

fundamental solution to the equation. Once this is found, solutions for arbitrary smooth initial conditions are obtained by convolution with the fundamental solution. With

$$\tilde{\phi}(0,k) = 1, \tag{7}$$

the solution is

$$\phi(t,x) = \frac{1}{(2\pi)^n} \int_{\tilde{X}} d^n k e^{-ik\cdot x} \exp(\tilde{\rho}(k)t), \tag{8}$$

with, for a kernel which only depends on the modulus of the distance ($\rho(|y-x|)$), in dimension n

$$\tilde{\rho}(k) = \tilde{\rho}(|k|) = (2\pi)^{n/2} \int dr r^{n-1} \rho(r) \frac{J_{\frac{n}{2}-1}(|k|r)}{(|k|r)^{\frac{n}{2}-1}}. \tag{9}$$

We will now particularize this solution for two types of kernels.

3.1. *The power-law case*

Let the connection strength be proportional to $\frac{c_1}{r^\beta}$ for most of the range of r. However, because this function is not normalizable, one truncates it with a $G(r)$ function

$$\begin{aligned} G(r) &= \begin{cases} 1, & \text{for } r_{\min} \le r \le r_{\max}\,, \\ 0, & \text{otherwise,} \end{cases} \\ \rho_1(r) &= \frac{c_1}{r^\beta} G(r), \end{aligned} \tag{10}$$

the normalization, $\int d^n x \rho_1(r) = 1$, implying

$$c_1 = \begin{cases} \dfrac{\Gamma(n/2)}{2\pi^{n/2}} \dfrac{n-\beta}{(r_{\max}^{n-\beta} - r_{\min}^{n-\beta})}, & (n \neq \beta), \\ \dfrac{\Gamma(n/2)}{2\pi^{n/2}} \left(\log \dfrac{r_{\max}}{r_{\min}}\right)^{-1}, & (n = \beta). \end{cases} \tag{11}$$

The asymptotic behavior for large times of the solution of Eq. (2) and its relation to the behavior of the Fourier transform $\tilde{\rho}_1(|k|)$ of $\rho_1(r)$ has been discussed by several authors in the past (see, for example, [21, 24]). Namely, the behavior of the solution for large times is controlled by the functional dependence of $\tilde{\rho}_1(|k|)$ at small $|k|$. In particular, if for small $|k|$

$$\tilde{\rho}_1(|k|) = 1 - A|k|^\alpha + o(|k|^\alpha), \tag{12}$$

then the large time asymptotic behavior of the solution is the same as for the solution $v(t,x)$ of the fractional Laplacian equation $\partial_t v(t,x) = -A(-\Delta)^{\alpha/2} v(t,x)$ with the same initial condition, namely

$$\lim_{t\to\infty} t^{n/\alpha} \max_x \{\phi(t,x) - v(t,x)\} = 0, \tag{13}$$

with an L^∞ rate of decay of the solution $t^{-n/\alpha}$. In particular for the $\alpha = 2$ case, the asymptotic behavior is identical to the heat equation with a decay rate $t^{-n/2}$ and the asymptotic profile is a Gaussian. Furthermore, refined asymptotics in terms of the derivatives of the fundamental solution, identical to those of the heat equation, were obtained [41]. What in principle would be of special importance for our network setting is also the fact that the same kind of estimate is obtained for nonlocal diffusion on a lattice [42]. All these are very interesting mathematical results, which however may not be very useful at relatively large, but finite, times. Let us compute the small $|k|$ behavior of the power-law Fourier transform $\tilde{\rho}_1(|k|)$

$$\begin{aligned}\tilde{\rho}_1(|k|) &= (2\pi)^{\frac{n}{2}} c_1 \int_{r_{\min}}^{r_{\max}} dr r^{n-1} \frac{J_{\frac{n}{2}-1}(|k|r)}{(|k|r)^{\frac{n}{2}-1}} \frac{1}{r^\beta} \\ &= 1 - A|k|^2 + \cdots, \end{aligned} \tag{14}$$

with

$$A = \begin{cases} \dfrac{n-\beta}{2n(n+2-\beta)} \dfrac{r_{\max}^{n+2-\beta} - r_{\min}^{n+2-\beta}}{r_{\max}^{n-\beta} - r_{\min}^{n-\beta}}, & \text{for } n \neq \beta, \\ \dfrac{1}{4n} \dfrac{r_{\max}^2 - r_{\min}^2}{\log r_{\max} - \log r_{\min}}, & \text{for } n = \beta. \end{cases} \tag{15}$$

According to the large time asymptotic results quoted above, the $\alpha = 2$ behavior of the small $|k|$ behavior of $\tilde{\rho}_1(|k|)$, might lead us to expect for this case a diffusion similar to the heat equation. This may indeed be true for extremely large times but not necessarily for the small or even relatively large times of practical importance. In any case the $\alpha = 2$ was to be expected, of course, because the $G(r)$ truncation makes $\rho_1(r)$ a compact support function [24].

The limited usefulness of the (14) expansion is already apparent from the fact that whenever the power-law range is large (large $|r_{\max} - r_{\min}|$) the A coefficient becomes very large. Then $\tilde{\rho}_1(|k|)$ decays with this rate only for a tiny fraction of $|k|$ which contributes little to the inverse Fourier transform $\phi(t, x)$ in (8). We illustrate this fact by numerically computing $\tilde{\rho}_1(|k|)$ in the $n = 2$, $\beta = 2$ case with $r_{\min} = 1$ and $r_{\max} = 200$ (Fig. 10).

One sees that the $\alpha = 2$ scaling only occurs for very small $|k|$. This is put in evidence by plotting in the same figure the line $1 - A|k|^2$. At around $|k| = 0.02$ there is a break for a quite different slope. We have numerically computed the slope α after the break for dimensions $n = 2$ to $n = 4$ and several β values. The results are plotted in Fig. 11 (left panel) which shows that they seem to follow a universal function of $(n - \beta)$. A rough fitting to a sigmoid function leads to $\alpha(n - \beta) \sim 2/(1 + \exp(\gamma(n - \beta + c)))$ with $\gamma = 1.5$ and $c = 1.1$.

In the right-hand side panel, we have plotted the factor B in the $\tilde{\rho}_1(|k|) \simeq 1 - B|k|^\alpha$ approximation with α as in the left-hand panel. The B coefficient has a weak dependence on n.

One sees that for large negative $n - \beta$ the power exponent is consistent with normal diffusion, but there is a large range of $n - \beta$ corresponding to anomalous

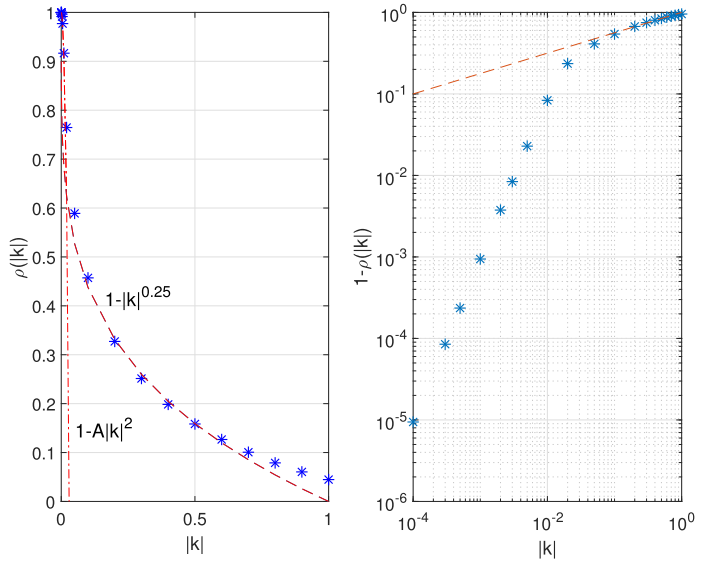

Fig. 10. $\tilde{\rho}(|k|)$ for the power-law case with $\beta = 2$, $n = 2$, $r_{\min} = 1$, $r_{\max} = 200$.

superdiffusion. This applies to intermediate times whereas, of course, for extremely large times the compact support nature of $\rho(r)$ restores the slope to the one of normal diffusion ($\alpha = 2$). As found above the dependence of the intermediate scaling factor is

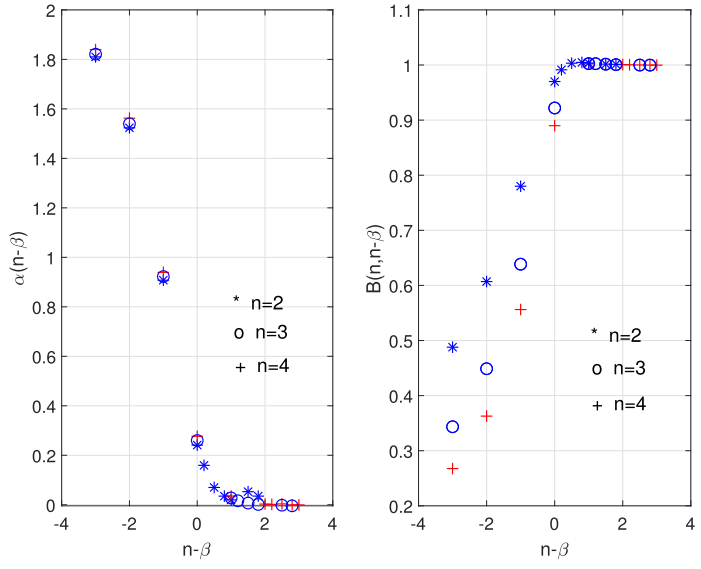

Fig. 11. The power exponent of the function $1 - \tilde{\rho}_1(|k|)$ after the break and the B coefficient in the $\tilde{\rho}_1(|k|) \simeq 1 - B|k|^{\alpha}$ approximation for intermediate large times.

far more complex than the one guessed from comparison with the Grunwald–Letnikov representation of the fractional derivative [18]. In conclusion:

For power-law powers β, such that $n - \beta \geq -1$ the nonlocal equation will display for intermediate large times a fractional superdiffusive behavior with exponent that follows an universal law as represented in Fig. 11. In Fig. 10, we have also plotted the function $1 - |k|^{\frac{1}{4}}$ to emphasize how this is a better first-order approximation as compared to the asymptotic $1 - A|k|^2$.

The configuration space solution $\phi_1(t, x)$ of (2) would be

$$\begin{aligned}\phi_1(t,r) &= \frac{1}{(2\pi)^{\frac{n}{2}}} \int_0^\infty d|k| \frac{|k|^{\frac{n}{2}}}{r^{\frac{n}{2}-1}} J_{\frac{n}{2}-1}(|k|r) e^{(\tilde{\rho}(|k|)-1)t} \\ &\simeq \frac{1}{(2\pi)^{\frac{n}{2}}} \left\{ \int_0^{|k|_b} d|k| \frac{|k|^{\frac{n}{2}}}{r^{\frac{n}{2}-1}} J_{\frac{n}{2}-1}(|k|r) e^{-A|k|^2 t} \right. \\ &\quad \left. + \int_{|k|_b}^\infty d|k| \frac{|k|^{\frac{n}{2}}}{r^{\frac{n}{2}-1}} J_{\frac{n}{2}-1}(|k|r) e^{-B|k|^\alpha t} \right\} \\ &\simeq \frac{1}{(2\pi)^{\frac{n}{2}}} \frac{1}{r^n} \int_{r|k|_b}^\infty dz z^{\frac{n}{2}} J_{\frac{n}{2}-1}(z) \exp\left(-Bz^\alpha \frac{t}{r^\alpha}\right). \end{aligned} \tag{16}$$

Therefore, for times not extremely large, the breaking point $|k|_b$ of the slope in $\tilde{\rho}_1(|k|)$ being very small, one concludes that $r^n \phi_1(t, r)$ is a function of $\frac{t}{r^\alpha}$

$$r^n \phi_1(t,r) \simeq \frac{1}{(2\pi)^{\frac{n}{2}}} \int_0^\infty dz z^{\frac{n}{2}} J_{\frac{n}{2}-1}(z) \exp\left(-Bz^\alpha \frac{t}{r^\alpha}\right). \tag{17}$$

This function is plotted in Figs. 12–14 for $n = 2, 3$ and 4. Note that the integral in (17) is ill-defined for $t/r^\alpha = 0$. It is a consequence of the initial condition of the fundamental solution being $\phi_1(0, x) = \delta^n(x)$.[d] Otherwise, as a function t/r^α, it provides a complete description of the time evolution of the fundamental solution. One notices a similar behavior for all dimensions, whenever the same $n - \beta$ is considered.

3.2. *The exponential case*

In the case

$$\rho_2(r) = c_2 e^{-\lambda r},$$

because of the fast decay of the exponential we may, to a good approximation, consider an infinite network. Then the normalization, $\int d^n x \rho_2(r) = 1$, implies for n dimensions

$$c_2 = \frac{\Gamma\left(\frac{n}{2}\right)}{\Gamma(n)} \frac{\lambda^n}{2\pi^{\frac{n}{2}}},$$

[d] In contrast to the case of the heat equation, there is in general no regularizing effect of the singular initial condition in the nonlocal diffusion equation, the fundamental solution being $e^{-t}\delta(x) + \phi(t, x)$ [24]. It is the smooth $\phi(t, x)$ part of the solution that is of interest for the study of signal propagation in the networks.

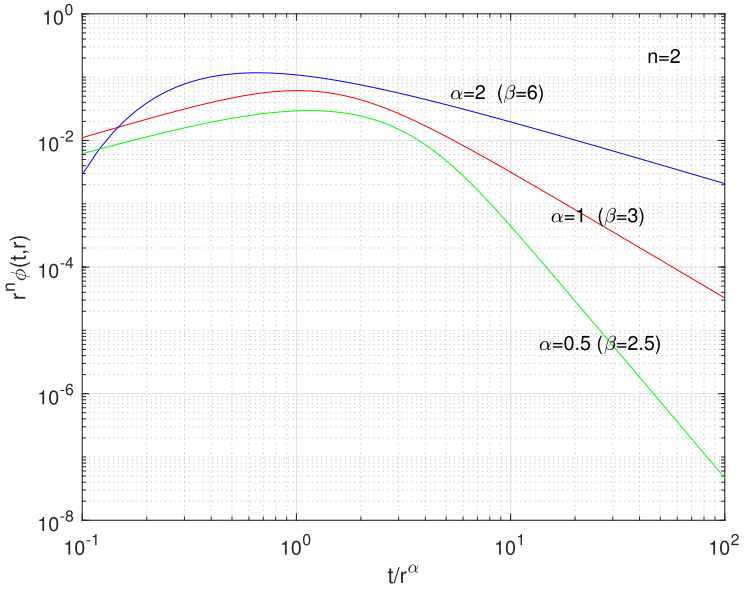

Fig. 12. The $r^n\phi(t,r)$ function in dimension 2 for the power-law case.

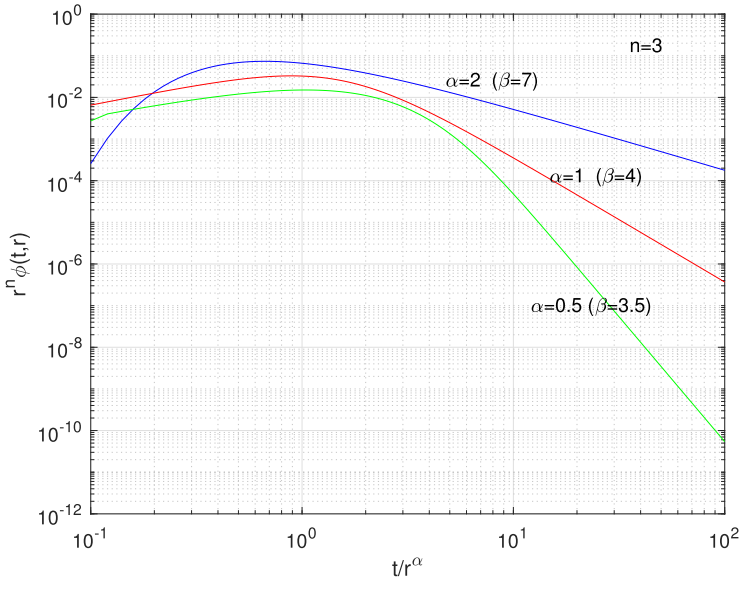

Fig. 13. The $r^n\phi(t,r)$ function in dimension 3 for the power-law case.

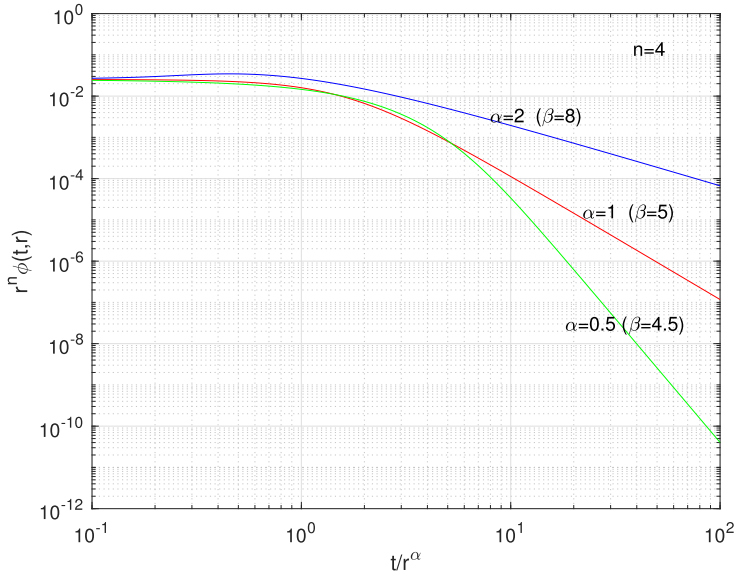

Fig. 14. The $r^n\phi(t,r)$ function in dimension 4 for the power-law case.

and the Fourier transform (5) of ρ_2 in dimension n is obtained in closed form

$$\tilde{\rho}_2(|k|) = \frac{\lambda^{n+1}}{(\lambda^2 + |k|^2)^{\frac{n+1}{2}}} = \frac{1}{\left(1 + \left(\frac{|k|}{\lambda}\right)^2\right)^{\frac{n+1}{2}}}.$$

and

$$\begin{aligned}\phi_2(t,r) &= \frac{1}{(2\pi)^{\frac{n}{2}}} \int_0^\infty d|k| \frac{|k|^{\frac{n}{2}}}{r^{\frac{n}{2}-1}} J_{\frac{n}{2}-1}(|k|r) \exp\left(\frac{\lambda^{n+1}}{(\lambda^2 + |k|^2)^{\frac{n+1}{2}}} - 1\right) t \\ &= \frac{1}{(2\pi)^n} \frac{1}{r^n} \int_0^\infty dz z^{\frac{n}{2}} J_{\frac{n}{2}-1}(z) \exp\left(\frac{1}{(1 + (z/\lambda r)^2)^{\frac{n+1}{2}}} - 1\right) t,\end{aligned}$$

$r^n\phi_2(t,r)$ being in this case a function of $(t, \lambda r)$. In Fig. 15, we have plotted the $|k|$ dependence of $\tilde{\rho}_2(|k|)$ and $1 - \tilde{\rho}_2(|k|)$.

One sees that for a large $|k|/\lambda$ region the slope of $1 - \tilde{\rho}_2(|k|)$ is similar to the one of normal diffusion. Hence, it is only for very small values of λ that one should expect anomalous diffusion effects. This is also clear from the size of the $|k|^2$ coefficient in the Taylor expansion of $\tilde{\rho}_2(|k|)$

$$\tilde{\rho}_2(|k|) = 1 - \frac{n+1}{2\lambda^2}|k|^2 + \cdots.$$

Therefore, propagation of information on the network is expected to be much less efficient than in the power-law case.

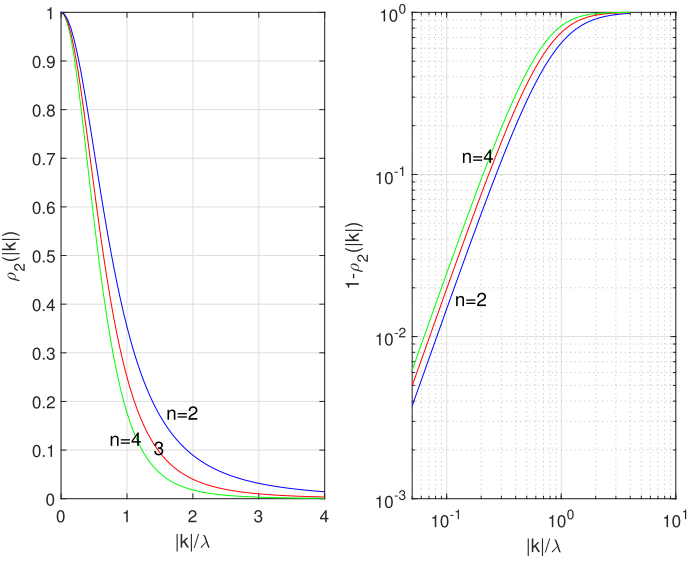

Fig. 15. The Fourier kernel $\rho_2(|k|)$ for the exponential case.

3.3. *Comparing the propagation of information in power-law and exponential networks*

Here, we compare by numerical simulation the propagation of information in power-law and in exponential networks. We consider a network of 40,000 agents placed on a 200×200 two-dimensional lattice and establish among them networks with unit connection strengths distributed according to a distance-dependent law, either a power law $p(d) = \frac{c_\alpha}{d^\alpha}$ or $p(d) = c_e e^{-d}$. These normalized probability functions are displayed in Fig. 16.

One sees that up to distance ≈ 10 the connection probabilities are not very different, but for larger distances they very much differ. The distance that is used in the lattice is the taxi metric $d_{AB} = |x_A - x_B| + |y_A - y_B|$.

The propagation experiments are performed in the following way: One chooses at random two distant agents in the network, the "source" A and the "destination" B. At the initial time there is a unit pulse at A that this agent is going to transmit with unit intensity to all its neighbors (meaning the agents that are connected to it, regardless of the physical distance). At the next time step, the neighbors that received the pulse do the same operation and so on. We use a no-cycle condition, that is, each agent transmits the pulse to its neighbors only once, even if it receives any other pulse later on. In this sense, we are not considering exactly the diffusion situation studied in Sec. 2 although the results are qualitatively the same. The process ends at a time when the destination B no longer receives any more pulses. This experiment has been repeated many times with very similar results every time. A typical result is shown in Fig. 17. The intensities represent the number of pulses

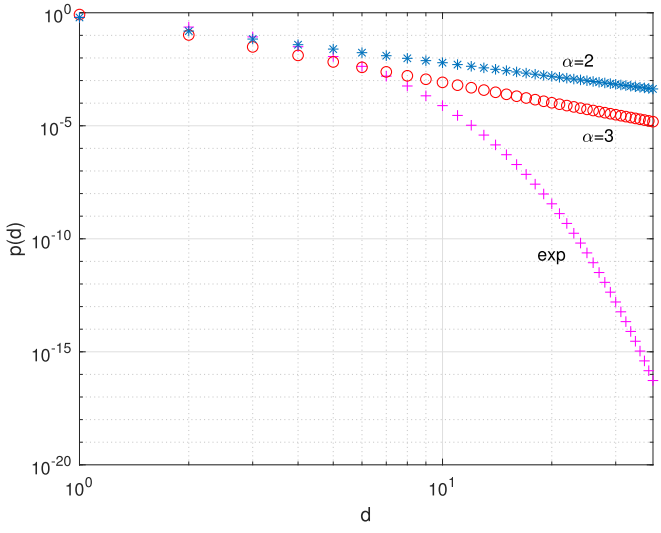

Fig. 16. Connection probabilities for power-law ($\alpha = 2$ and 3) and exponential networks.

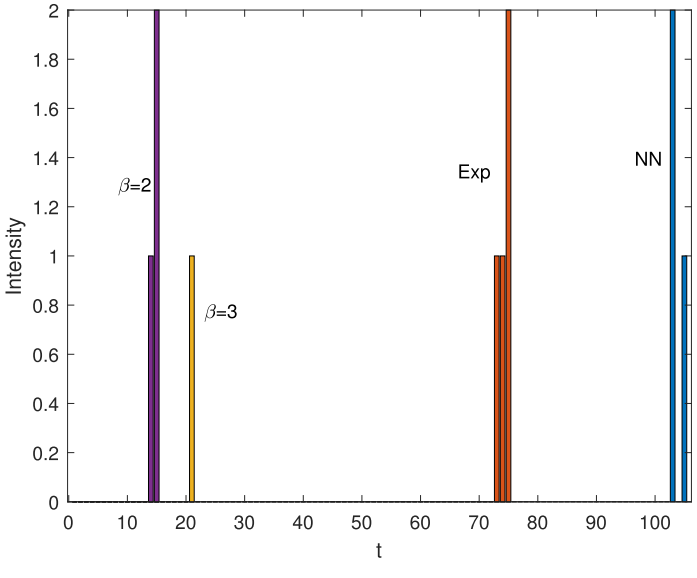

Fig. 17. A typical result of the propagation of information experiment with power-law ($\alpha = 2$ and 3), exponential and nearest-neighbor networks.

received at each time. We have also compared the speed of propagation with a nearest-neighbor network. All networks have the same number of connections (79,600). The conclusion is that power-law networks, with the same number of connections, are extremely more efficient in the propagation of information than the

others. Although better than the nearest-neighbor one, the exponential network fares poorly.

Acknowledgment

The authors acknowledge financial support from FCT — Fundação para a Ciência e Tecnologia (Portugal) through research grants UIDB/04561/2020 and UIDB/05069/2020.

References

[1] Park, H.-J. and Friston, K., Structural and functional brain networks: From connections to cognition, *Science* **342** (2013) 1238411.
[2] Wig, G. S., Schlaggar, B. L. and Petersen, S. E., Concepts and principles in the analysis of brain networks, *Ann. New York Acad. Sci.* **1224** (2011) 126–146.
[3] Knösche, T. R. and Tittgemeyer, M., The role of long-range connectivity for the characterization of the functional–anatomical organization of the cortex, *Front. Syst. Neurosci.* **5** (2011) 58.
[4] Betzel, R. F. and Bassett, D. S., Specificity and robustness of long-distance connections in weighted, interareal connectomes, *Proc. Natl. Acad. Sci. USA* **115** (2018) E4880–E4889.
[5] Padula, M. C., Schaer, M., Scariati, E., Mutlu, A. K., Zöller, D., Schneider, M. and Eliez, S., Quantifying indices of short- and long-range white matter connectivity at each cortical vertex, *PLoS One* **12** (2017) 0187493.
[6] Drawitsch, F., Karimi, A., Boergens, K. M. and Helmstaedter, M., FluoEM, virtual labeling of axons in three-dimensional electron microscopy data for long-range connectomics, *eLife* **7** (2018) e38976.
[7] Barttfeld, P. *et al.*, Organization of brain networks governed by long-range connections index autistic traits in the general population, *J. Neurodev. Disord.* **5** (2013) 16.
[8] Hogan, B., Visualizing and interpreting Facebook networks, in *Analysing Social Media Networks with NodeXL*, Hansen, D. L. *et al.* (ed.) (Elsevier, 2011), pp. 165–179.
[9] Billedo, C. J., Kerkhof, P. and Finkenauer, C., The use of social networking sites for relationship maintenance in long-distance and geographically close romantic relationships, *Cyberpsychol. Behav. Soc. Netw.* **18** (2015) 152–157.
[10] Carvalho, R. and Iori, G., Socioeconomic networks with long-range interactions, *Phys. Rev. E* **78** (2008) 016110.
[11] Gustafson, K. B., Bayati, B. S. and Eckhoff, P. A., Fractional diffusion emulates a human mobility network during a simulated disease outbreak, *Front. Ecol. Evol.* **5** (2017) 35.
[12] Riascos, A. P. and Mateos, J. L., Fractional dynamics on networks: Emergence of anomalous diffusion and Lévy flights, *Phys. Rev. E* **90** (2014) 032809.
[13] Riascos, A. P., Michelitsch, T. M., Collet, B. A., Nowakowski, A. F. and Nicolleau, F. C. G. A., Random walks with long-range steps generated by functions of Laplacian matrices, *J. Stat. Mech., Theory Exp.* **2018** (2018) 043404.
[14] Estrada, E., Delvenne, J.-C., Hatano, N., Mateos, J. L., Metzler, R., Riascos, A. P. and Schaub, M. T., Random multi-hopper model: Super-fast random walks on graphs, *J. Complex Netw.* **6** (2018) 382–403.
[15] Weng, T., Zhang, J., Khajehnejad, M., Small, M., Zheng, R. and Hui, P., Navigation by anomalous random walks on complex networks, *Sci. Rep.* **6** (2016) 37547.

[16] de Nigris, S., Carletti, T. and Lambiotte, R., Onset of anomalous diffusion from local motion rules, *Phys. Rev. E* **95** (2017) 022113.
[17] Vilela Mendes, R., Fractional networks, the new structure, *Chaos Complex. Lett.* **12** (2018) 123–128, arXiv:1804.10605.
[18] Vilela Mendes, R. and Araújo, T., Long-range connections and mixed diffusion in fractional networks, preprint (2020), arXiv:2002.04351.
[19] Barthélemy, M., Spatial networks, *Phys. Rep.* **499** (2011) 1–101.
[20] Broido, A. D. and Clauset, A., Scale-free networks are rare, *Nat. Commun.* **10** (2019) 1017.
[21] Andreu-Vaillo, F., Mazón, J. M., Rossi, J. D. and Toledo-Melero, J. J., *Nonlocal Diffusion Problems*, Mathematical Surveys and Monographs, Vol. 165 (American Mathematical Society, Providence, 2010).
[22] Bucur, C. and Valdinoci, E., *Nonlocal Diffusion and Applications* (Springer, Switzerland, 2016).
[23] Vázquez, J. L., The mathematical theories of diffusion: Nonlinear and fractional diffusion, in *Nonlocal and Nonlinear Diffusions and Interactions: New Methods and Directions*, Lecture Notes in Mathematics, Vol. 2186 (Springer, Cham, 2017), pp. 205–278.
[24] Chasseigne, E., Chaves, M. and Rossi, J. D., Asymptotic behavior for nonlocal diffusion equations, *J. Math. Pures Appl.* **86** (2006) 271–291.
[25] Kleinberg, J. M., Navigation in a small world, *Nature* **406** (2000) 845.
[26] Li, C. and Ma, W., Synchronizations in complex fractional networks, in *Handbook of Fractional Calculus with Applications*, Petrás, I. (ed.), Vol. 6 (Walter de Gruyter, Berlin, 2019), pp. 379–396.
[27] Zuñiga Aguilar, C. J. *et al.*, Fractional order neural networks for system identification, *Chaos Solitons Fractals* **130** (2020) 109444.
[28] https://www.transtats.bts.gov.
[29] Viana, M. P. and Costa, L. F., Fast long-range connections in transportation networks, *Phys. Lett. A* **375** (2011) 1626–1629.
[30] González, M. C., Hidalgo, C. A. and Barabási, A.-L., Understanding individual human mobility patterns, *Nature* **453** (2008) 779–782.
[31] Riascos, A. P. and Mateos, J. L., Networks and long-range mobility in cities: A study of more than one billion taxi trips in New York City, *Nat. Sci. Rep.* **10** (2020) 4022.
[32] Markov, N. T., Ercsey-Ravasz, M. M., Lamy, C., Gomes, A. R. R., Magrou, L., Misery, P., Giroud, P., Barone, P., Dehay, C., Toroczkai, Z., Knoblauch, K., Van Essen, D. C. and Kennedy, H., The role of long-range connections on the specificity of the macaque interareal cortical network, *Proc. Natl. Acad. Sci. USA* **110** (2013) 5187–5192.
[33] Markov, N. T. *et al.*, A weighted and directed interareal connectivity matrix for macaque cerebral cortex, *Cereb. Cortex* **24** (2014) 17–36.
[34] Gamanut, R., Kennedy, H., Toroczkai, Z., Van Essen, D., Knoblauch, K. and Burkhalter, A., The mouse cortical connectome characterized by an ultra-dense cortical graph maintains specificity by distinct connectivity profiles, *Neuron* **97** (2018) 698–715.
[35] Horvat, S., Gamanut, R., Ercsey-Ravasz, M., Magrou, L., Gamanut, B., Van Essen, D. C., Burkhalter, A., Knoblauch, K., Toroczkai, Z. and Kennedy, H., Spatial embedding and wiring cost constrain the functional layout of the cortical network of rodents and primates, *PLoS Biol.* **14** (2016) e1002512.
[36] Ercsey-Ravasz, M. *et al.*, A predictive network model of cerebral cortical connectivity based on a distance rule, *Neuron* **80** (2013) 184–197.
[37] Knox, J. E. *et al.*, High-resolution data-driven model of the mouse connectome, *Netw. Neurosci.* **3** (2018) 217–236.

[38] Rossi, R. A. and Ahmed, N. K., The network data repository with interactive graph analytics and visualization (2015), http://networkrepository.com.
[39] https://www.cs.cornell.edu/126 arb/data/spatial-fungi/.
[40] Lee, S. H., Fricker, M. D. and Porter, M. A., Mesoscale analyses of fungal networks as an approach for quantifying phenotypic traits, *J. Complex Netw.* **5** (2017) 145–159.
[41] Ignat, L. I. and Rossi, J. D., Refined asymptotic expansions for nonlocal diffusion equations, *J. Evol. Equ.* **8** (2008) 617–629.
[42] Ignat, L. I. and Rossi, J. D., Asymptotic behaviour for a nonlocal diffusion equation on a lattice, *Z. Angew. Math. Phys.* **59** (2008) 918–925.